A Study of Performance and Complexity for IEEE 802.11n MIMO-OFDM GIS Solutions

M. K. Abdul Aziz and A.R. Nix
Centre for Communications Research,
University of Bristol,
Merchant Venturers Building, Woodland Road,
Bristol, BS8 1UB, UK
E-mail: {M.K.Abdulaziz, Andy.Nix}@bristol.ac.uk

P.N. Fletcher
QinetiQ Ltd,
St. Andrews Road,
Malvern,
Worcestershire, WR14 3PS, UK
E-mail: Pnfletcher@qinetiq.com

Abstract—**This paper investigates the point-to-point PHY layer performance of two newly proposed IEEE 802.11n candidate solutions by suggesting extensions to 802.11a. The new solutions incorporate a MIMO architecture for the wireless links between the network terminals. The FEC block in the PHY layer chain is enhanced with a Turbo encoder to provide interleaving gains for the larger sized PSDUs (1-4095 bytes). Due to the ambitious data rate targets identified in 802.11n, where 'on-air' data rates of 108-320Mbit/s are quoted, a large MIMO architecture comprising 6 Transmit and 6 Receive antenna elements is adopted. ML detection using such large configurations is often prohibitively complex due to an unrealistic enumerated symbol list. In this paper we propose ZF-GIS and MMSE-GIS solutions to ease complexity at the receiver. The PER performance offered by both proposals is compared together with the added computational requirements in constructing their matrices. Link throughputs are compared to demonstrate the viability of the chosen solutions.**

Keywords - 802.11a; 802.11n; MIMO; MMSE-GIS; ZF-GIS

I. INTRODUCTION

In recent years, advancements in the field of wireless communications have generated great interest in the deployment of multiple element antenna arrays for mobile terminals. These methods have the potential to dramatically increase both performance and capacity [1]. The list for Multiple Input Multiple Output (MIMO) diversity enhancing techniques are well known and range from simple transmit delay diversity schemes to hand designed Space Time Trellis Coded (STTC) solutions [5]. Further combinatorial schemes for MIMO architectures with Turbo decoding are discussed in [3] as it has shown exceptional performance [4] when adopted for conventional Single Input Single Output (SISO) configurations. This led to the study presented in [10], where Turbo codes were incorporated into the design of STTC for QAM constellations.

In order to maintain a positive outlook for future generations of WLAN, the 802.11n (High Throughput Task group) was established to look into the use of multiple antennas as possible solutions to provide very high data throughputs [3], reaching peak values of up to 320Mbit/s.

In this paper, we present future PHY layer performance results for an 802.11n candidate based on an extended version of the 802.11a PHY layer chain [2]. The use of multiple antennas at the transmitter is proposed to support the spatial multiplexing of independent PHY bursts. The convolutional code FEC in 802.11a is replaced here with Turbo codes to provide an interleaving gain for superior performance with larger sized Physical Service Data Units (PSDUs). At the receiving terminals, the signals are detected via a sub-optimal Maximum Likelihood (ML) solution in conjunction with Minimum Mean Squared Error (MMSE) and Zero Forcing Group Interference Suppressions (GIS). These methods are used to reduce the symbol enumerated search list. The calculated Log-Likelihood Ratio (LLR) observations are fed into an iterative decoder and a hard decision is made to retrieve the original binary information sent in the payload. Another motivation for this paper is to investigate the additional computational overhead of constructing ZF-GIS and MMSE-GIS matrices. Although it is widely known that the MMSE solution will yield an expected improvement over the ZF-GIS, it also incurs a larger complexity cost. Hence, a detailed description of the necessary computational processes is useful for determining which method offers the better complexity/performance trade-off. This issue is even more critical in spatially multiplexed MIMO-OFDM, since each data bearing subcarrier (assuming independent fades across the spectrum of interest) requires an equal amount of computational complexity.

The paper is organized as follows. Section II describes the MIMO description for OFDM. Section III explains the GIS solutions utilized for partial ML decoding and section IV details the arithmetic operations involved for construction of these GIS matrices. Finally, the paper concludes by comparing and discussing the performance of the MIMO architectures as a potential solution for 802.11n.

II. THE MIMO-OFDM DESCRIPTION

In a MIMO architecture with m transmit antennas, individual PHY bursts are sent simultaneously from each antenna element. Therefore, a matrix of size m by M_c bits must be constructed at the transmitter and this is then mapped to symbols for each subcarrier, k, where M_c represents the number of bits per subcarrier. This is represented as shown in equation 1, where the Gray coded constellation mapping is imposed on the rows of $\boldsymbol{b_k}$.

This research was sponsored by QinetiQ Ltd.

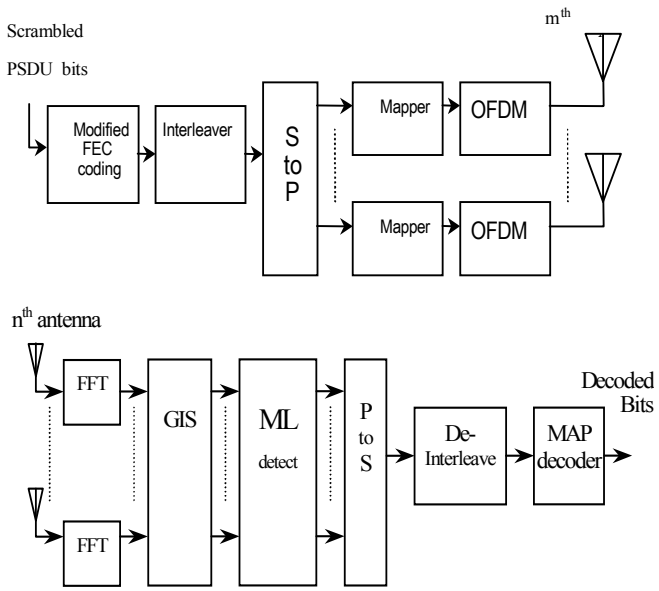

Figure 1: MIMO architectures applied to IEEE 802.11n candidate Transmitter and Receiver.

$$\boldsymbol{b_k} = \begin{bmatrix} b_{1,1} & b_{1,2} & \cdots & b_{1,M_c} \\ b_{2,1} & b_{2,2} & \cdots & b_{2,M_c} \\ \vdots & \vdots & \ddots & \vdots \\ b_{m,1} & b_{m,2} & \cdots & b_{m,M_c} \end{bmatrix} \quad (1)$$

The IEEE 802.11a standard allocates a bandwidth (including guard bands), B_W, of 20MHz and an OFDM symbol period (including cyclic prefix), T_s, of 4μs. This results in a nominal bit rate that increases linearly with the number of transmit antennas deployed. At the receiver, the cyclic prefixes are removed and an FFT is performed for the data received on each antenna element. The receiver architecture is shown in fig. 1.

Since the FFT is a linear process, the extracted frequency domain data can be represented as summations of the transmitted symbols at a given subcarrier for all m transmit antennas. This is given as:

$$R_{k,i} = \sum_{j=1}^{m} H_{k,i,j} C_{k,j} + \eta_{k,i} \,. \quad (2)$$

In a more compact form, (2) can be equivalently represented as:

$$\boldsymbol{R_k} = \boldsymbol{H_k C_k} + \boldsymbol{\eta_k} \quad (3)$$

where

$$\boldsymbol{R_k} = [R_{k,1} \quad R_{k,2} \quad \cdots \quad R_{k,n}]^T \quad (4)$$

$$\boldsymbol{C_k} = map(\boldsymbol{b_k}) = [C_{k,1} \quad C_{k,2} \quad \cdots \quad C_{k,m}]^T \quad (5)$$

$$\boldsymbol{\eta_k} = [\eta_{k,1} \quad \eta_{k,2} \quad \cdots \quad \eta_{k,n}]^T \quad (6)$$

$$\boldsymbol{H_k} = \begin{bmatrix} H_{k,1,1} & H_{k,1,2} & \cdots & H_{k,1,m} \\ H_{k,2,1} & H_{k,2,2} & \cdots & H_{k,2,m} \\ \vdots & \vdots & \ddots & \vdots \\ H_{k,n,1} & H_{k,n,2} & \cdots & H_{k,n,m} \end{bmatrix} \quad (7)$$

with T denoting the matrix transpose and $H_{k,i,j}$ representing the channel values from transmit antenna j; $1 \le j \le m$ to receive antenna i; $1 \le i \le n$ for each of the data bearing subcarriers k; $-26 \le k \le 26$, $k \ne \{-21,-7,0,7,21\}$. $C_{k,j}$ represents the frequency domain mapped data symbols and $\eta_{k,i}$ are independent complex valued Gaussian noise samples of zero mean and variance per dimension σ^2.

Based on the received subcarriers, $\boldsymbol{R_k}$ and the Channel State Information (CSI) vector, which is obtained from the predefined SC-preamble for each corresponding subcarrier, the bit LLRs are computed by enumerating across all the possible mapped symbols for all transmit antennas.

$$P[b_{p,q} \mid \boldsymbol{R}] = \sum_{\boldsymbol{C}:\boldsymbol{C}=map(\boldsymbol{b})} \prod_{i=1}^{n} \exp\left(- \frac{\left| R_i - \sum_{j=1}^{m} H_{i,j} C_j \right|^2}{2\sigma^2} \right) \quad (8)$$

Summing over all conditional probabilities (enumerated list of possible symbols) and taking into account the independence of the signals between receive antennas due to uncorrelated channel fades; we obtain bit level conditional probabilities given by equation (8), where each sent symbol bears the same probability of transmission and the received signals are corrupted by AWGN with a variance per dimension of σ^2. Equation (8) becomes the basis for our ML detector and for the generation of LLRs prior to the iterative MAP decoder.

III. GIS SOLUTIONS

Due to the large MEA architectures proposed in this paper, the list of probable symbols sent for LLR calculation per binary bit becomes unrealistic for real time execution in hardware. Hence, as in [7,12], we propose to use the ZF-GIS and MMSE-techniques to limit this enumeration list to be exponential in E_c rather than m, where E_c is referred to as the *enumeration constant*. A zero forcing solution is always possible in symmetric MIMO configurations with independent channel fades since the process of grouping interferers will inevitably introduce rank deficient matrices. Therefore, there always exists a collection of *non*-unique vectors that result in the inner product result given by equation (9).

$$\boldsymbol{W}_{zf}{}^{H}\,[\,H_{des} \quad H_{\text{int}}\,] = [\,\hat{\boldsymbol{H}} \quad \boldsymbol{0}\,] \qquad (9)$$

where $\boldsymbol{W}_{zf}$ is the set of vectors that project the group of interferers, $\boldsymbol{H}_{int}$ into its *Nullspace* and ^{H} is the notation for a *Hermitian* transpose. The effects from the desired signal contributors form $\boldsymbol{H}_{des}$, the collection of columns that correspond to the particular transmitted symbols of interest such that the channel matrix is actually:

$$\boldsymbol{H} = [\,H_{des} \quad H_{\text{int}}\,] \ . \qquad (10)$$

Since the zero forcing solution is the set of vectors that exist in a subspace orthogonal to $\boldsymbol{H}_{int}$, these vectors can be found by reflecting themselves upon $\boldsymbol{H}_{des}$. This is given as:

$$\boldsymbol{W}_{zf} = \left\{\left[\boldsymbol{I} - \boldsymbol{H}_{int}\left(\boldsymbol{H}_{int}{}^{H}\boldsymbol{H}_{int}\right)^{-1}\boldsymbol{H}_{int}{}^{H}\right]\right\} \qquad (11)$$

However, since ZF-GIS suppression fails to take into account noise statistics in its solution, the complete suppression of interferers runs the risk of noise amplification.

$$\boldsymbol{W}_{mmse} = \left\{\left[\left(\frac{\boldsymbol{P_T}}{\boldsymbol{m}}\right)\boldsymbol{H}\boldsymbol{H}^{H} + \sigma^2\boldsymbol{I}\right]^{-1}\left(\frac{\boldsymbol{P_T}}{\boldsymbol{m}}\right)\boldsymbol{H}\overline{\boldsymbol{H}}_{\boldsymbol{des}}{}^{H}\right\} \qquad (12)$$

The MMSE-GIS offers a trade-off in the suppression of interferers and noise. Based on the *Wiener-Hopf* solution for minimization of error (a function of both noise and interferers), the MMSE-GIS tap weights are given as shown in (12). Here, $\overline{\boldsymbol{H}}_{des}$ is constructed by zeroing out columns occupied by $\boldsymbol{H}_{int}$. Therefore, ignoring the suppressed interferers by applying the ZF-GIS or MMSE-GIS tap weights, generalized as $\boldsymbol{W}$, to $\boldsymbol{R}_k$, as in (9), the GIS solutions for conditional bit probabilities become:

$$P[b_{p,q} \mid \hat{\boldsymbol{R}}] = \sum_{\boldsymbol{C}:\boldsymbol{C}=map(\boldsymbol{b})}\prod_{i}\exp\left(-\frac{\left|\hat{R}_i - \sum_{j}\hat{H}_{i,j}C_j\right|^2}{2\sigma^2}\right) \qquad (13)$$

where

$$\hat{\boldsymbol{R}} = \boldsymbol{W}^{H}\boldsymbol{R} \qquad (14)$$

We observe that the values are KE_c-E_c+1 $\le i \le KE_c$ and $1 \le j \le n$. K is the number of suppressions required in order to fully account for all the signals transmitted in each frequency slot occupied by an individual subcarrier. This reflects the reduction in the size of the candidate list for a more realistic ML solution.

IV. GIS Matrices Computation

In this section we detail the GIS computations for the construction of the MMSE-GIS and ZF-GIS solutions. Since both matrix constructions entail a matrix inversion, an analysis of this process is required. Assuming that the channel matrix is full rank and square, it is possible to implement this matrix inversion by solving for an identity matrix using forward and backward substitutions of an upper and lower triangularised channel matrix. This can be achieved by applying the LU factorization to the channel matrix. By breaking down the Outer Product Gaussian Elimination algorithm, as in [11], the triangularisation process is an iterative procedure that requires complex division, subtraction and the calculation of an outer matrix product. In backwards substitution, values are determined through an iterative decision and cancellation process. Computation for the forward substitution will require an equivalent complexity. In terms of real operations, the list of mathematical operations is given in table 1. Note that in this paper only square matrices are considered and hence the value of *n* equals *m*.

TABLE I. MATRIX INVERSION: REAL OPERATIONS

Processes	Operations	
	LU	Forward and Backward Substitution
Multiplies	$\sum_{k=1}^{n-1}10(n-k)$	$\left[\sum_{k=1}^{n-1}8(k+1)\right]+12n$
Adds	$\sum_{k=1}^{n-1}5(n-k)$	$\left[\sum_{k=1}^{n-1}4(k+1)+4k\right]+6n$
Subtracts	$\left[\sum_{k=1}^{n-1}2(n-k)+2(n-k)^2\right]$	$\left[\sum_{k=1}^{n-1}2(k+1)\right]+6n$
Divides	$\sum_{k=1}^{n-1}(n-k)$	$2n$

In conditions where the channel matrix suffers from rank deficiency, a partial pivot can be applied with similar complexity. This is because the partial pivot only involves interchanging rows and can be described by a row permuting matrix.

For the case of the ZF- GIS, we translate the interfering components of the channel into its orthogonal subspace. This requires a matrix inversion together with inner and outer matrix multiplications. In the case of MMSE-GIS value calculations, more operations are necessary to include the signal power and noise variance. Including the cost of the matrix inversion, the total number of operations required for the construction of these matrices is given in table II. Assuming that all the arithmetic involved is executed as floating point operations, the flop count can be obtained by simply adding up all of the described operations.

TABLE II. GIS MATRIX CONSTRUCTION: REAL OPERATIONS

Processes	Operations	
	ZF GIS	MMSE GIS
Multiplies	$12n^3 - 20n^2E_c + 8nE_c^2 + 12n + \sum_{k=1}^{n-1}(10n - 2k + 8)$	$8n^3 + 4n^2 + 4n^2E_c + 14n + \sum_{k=1}^{n-1}(10n - 2k + 8)$
Adds	$10n^3 - 16n^2E_c + 6nE_c^2 + 6n + \sum_{k=1}^{n-1}(5n + 3k + 4)$	$8n^3 + 4n^2E_c + 8n + \sum_{k=1}^{n-1}(5n + 3k + 4)$
Subtracts	$3n^3 + n^2 - 5n^2E_c + 2nE_c + 6n + \sum_{k=1}^{n-1}(2n^2 - 4nk + 2n + 2k^2 + 2)$	$2n^3 + n^2E_c + 6n + \sum_{k=1}^{n-1}(2n^2 - 4nk + 2n + 2k^2 + 2)$
Divides	$2n + \sum_{k=1}^{n-1} n - k$	$2n + \sum_{k=1}^{n-1} n - k$

V. SIMULATION SETUP

It is proposed that the encoder be replaced by two parallel concatenated RSC encoders. The first encoder will be fed with the information bits, whereas the second encoder is fed with an interleaved version of the same bits. The interleaver is pseudo-random. Terminating tail bits are appended to the PSDU bits to return the first RSC encoder to its zero state. The FEC coded bits are fed through the standard block interleaver before multiplexing to assign each bit to its respective transmit antenna. The (Gray) mapped symbols undergo an IFFT process that converts the frequency symbols into the time domain.

The RSC encoders are described by [1, g_1/g_2], where the forward and feedback generator polynomials are given as $g_1=\{5_8\}$ and $g_2=\{7_8\}$ respectively. The payload for each PHY burst is 162 bytes long. These lengths enable an integer number of OFDM symbols to be sent per PHY burst at each transmitting antenna element. The receivers are ZF-GIS and MMSE-GIS with partial ML detectors. Based on the assumption that the channel remains invariant throughout the MAC frame, the calculation of the GIS filter tap weights are calculated for every individual data bearing subcarrier per GIS grouping. Here an enumeration constraint, E_c of 2 is used with K=3 being the number of GIS groupings to account for all 6 transmitted symbols

The decoder employs a MAP algorithm to realize an iterative decoding solution where hard decisions are made after 8 iterations. ETSI Channel model 'A' is assumed in these simulations [8]. All results are based on PHY bursts sent over 1000-5000 independent realisations of the channel model. The channel impulse response taps for the spatially separated terminals are subject to independent and uncorrelated Rayleigh fading. In the MIMO architecture, the overall transmit power is normalized to be equivalent to the 802.11a SISO case.

Similarly, a MIMO 2x2 scenario is also presented that utilizes RSC encoders, $g_1=\{21_8\}$ and $g_2=\{37_8\}$. More rigorous decoding is applied where hard decisions are obtained after 10 iterations. The payloads for these PHY bursts are between 144 and 180 bytes long. Only the ML approach is used for decoding. In this configuration, more processing power is allocated to the decoding stage but at the sacrifice of increased throughput, as seen in the 6x6 case. The enumeration list for the ML and GIS solutions are also equivalent.

VI. RESULTS

In this section, results are presented for the techniques discussed in section III of this paper. Under the assumption that each packet uses the Cyclic Redundancy Check for error detection, if no acknowledgment is received then the terminal will retransmit the packet [6]. Assuming an ideal Link Adaptation, the mode with the highest throughput is always chosen, the data throughput is approximated as [9]:

$$T_L = \Re_{ext}\ (1 - PER) \qquad (15)$$

where $\Re_{ext}$ represents the bit rate and PER denotes the Packet Error Rate for a specific PHY layer mode. MAC overheads are not accounted for in this approximation.

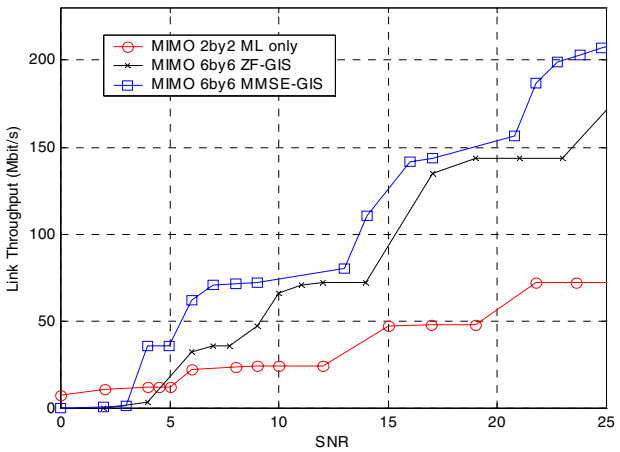

Figure 2: Proposed IEEE 802.11n Link Throughputs with Link Adaptation for ML, MMSE and ZF-GIS solutions in ETSI channel 'A'.

From figure 2, we observe that the link throughput for the MMSE-GIS outperforms both the ZF-GIS solution and the complete ML approach for SNR values beyond 3dB. For SNR values less than 3dB, the ML solution for the 2Tx-2Rx architecture achieves the higher link throughput compared with the GIS solutions.

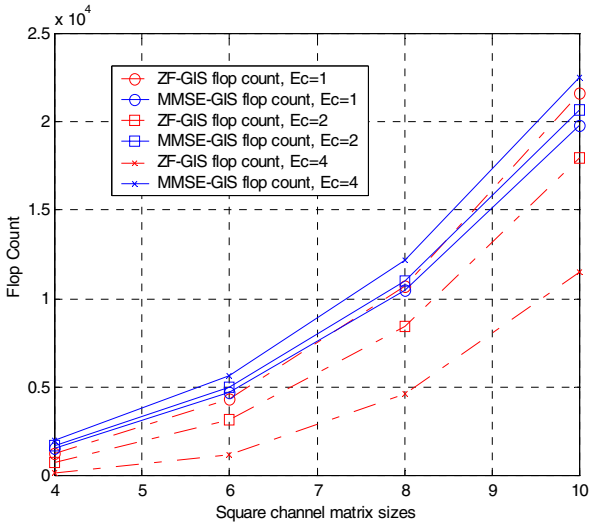

Figure 3: Flop count comparison for the construction of MMSE-GIS and ZF-GIS with different MIMO sizes and Enumeration constant, E_c.

Results presented in figure 3 emphasize the prediction that the MMSE-GIS matrix construction incurs a higher computational cost. For our proposed scenario with an E_c of 2, the ZF-GIS and MMSE-GIS require a flop count of 3124 and 4984 respectively. For a MIMO channel of size 10, the ZF-GIS needs 21616, 17956 and 11476 flops whereas the MMSE-GIS requires 19796, 20696 and 22496 flops for E_c of 1,2 and 4 respectively. It has also been shown that higher values of E_c will give higher complexity for the MMSE-GIS, but that this lowers the complexity for the ZF-GIS solution. This is because the requirement imposed on equation (11) decreases with increasing E_c.

VII. Conclusions

This paper has studied the application of multiple transmit and receive antennas for WLANs and proposed a new solution for IEEE 802.11n that is a logical extension of the 802.11a standard. The analysis was performed using the ETSI/IEEE specified indoor typical NLOS channel model. The Link Throughput and processing complexity were presented for each of the 802.11n solutions proposed in this paper.

It was shown that for the ML solution with 2 transmit and 2 receive antennas, iterative turbo decoding offers more reliable performance at low SNRs compared to the GIS solutions presented here. Although it did not require any additional complexity in providing the LLR ratio, it incurred a higher complexity in its decoding block. However even with a more robust decoding block, results have shown that the link throughput performance for ZF-GIS and MMSE-GIS gave improved performances beyond 5dB.

This paper also broken down the computations involved for generating the GIS solutions for complex channel matrices. In general, the MMSE-GIS solution will require more computations compared to the ZF-GIS solution for E_c of 2 and 4 and at any given channel matrix size. However at an E_c of 1, the complexity of both solutions is very similar. This makes the MMSE-GIS solution more attractive for small values of E_c. Assuming that time invariance is maintained throughout a MAC frame, the GIS tap filter weights can be calculated per individual subcarrier for each grouping. Hence each PHY burst would require 144 GIS solutions in addition to the reduced enumerated list for the sub-optimal ML solution.

In conclusion, incorporating large MIMO architectures with iterative decoding is realizable when a GIS solution is applied. This is due to the long enumeration list involved in an ML solution. It has been shown that for low values of E_c, the MMSE-GIS becomes attractive due to its superior performance compared to the ZF-GIS. However for higher values of E_c the ZF-GIS requires a smaller number of flops for implementation. We conclude that it is desirable to allow additional complexity in the design of the 802.11n network terminals in order to realize a spatial multiplexing solution.

Acknowledgments

The authors wish to acknowledge the financial and technical support of QinetiQ Ltd. They also thank Dr. A. Doufexi and Dr. M. Butler for assistance and support with the 802.11n simulations.

References

[1] G.J. Foschini and M. Gans, 'On limits of wireless communications in a fading environment when using multiple antennas', Wireless Personal Communications, Vol. 6, pp. 311-335, 1998.

[2] V. Tarokh, N. Seshadri and A. Calderbank, 'Space-time codes for high data rate wireless communication - performance criterion and code construction', IEEE Trans. on Information Theory, Vol. 44, no. 2, pp. 744-765, March 1998.

[3] S. L. Ariyavisitakul, 'Turbo space-time processing to improve wireless channel capacity', IEEE Transactions on Communications, Vol. 48, pp. 1347–1359, Aug 2000.

[4] C. Berrou, A. Glavieux and P. Thitimajshima, 'Near Shannon limit error-correcting coding and decoding: Turbo codes', Proc. 1993 Int. Conf. Comm, pp 1064-1070, 1993.

[5] Y. Liu, P. Fitz and O. Takeshita, 'A full rate space-time turbo codes', IEEE JSAC, Vol. 19, no. 5, pp. 969-980, May 2001.

[6] IEEE Std 802.11a/D7.0-1999, Part11: Wireless LAN Medium Access Control (MAC) and Physical Layer (PHY) specifications: High Speed Physical Layer in the 5GHz Band, 1999.

[7] A. Stefanov and T. Duman, 'Turbo-coded modulation for systems with transmit and receive antenna diversity over block fading channels: system model, decoding approaches, and practical considerations', IEEE JSAC, Vol. 48, pp. 1347-1359, Aug. 2000.

[8] J. Medbo and P. Schramm, 'Channel Models for HIPERLAN/2', ETSI/BRAN document no. 3ERI085B, 1998.

[9] M.K. Abdul Aziz, P.N. Fletcher and A.R. Nix, 'Extension to the IEEE 802.11a standard incorporating iterative turbo decoding with transmit delay diversity', WPMC 2002, Oct. 2002.

[10] A. Doufexi, S. Armour, M. Butler, A. Nix and D. Bull, 'A Study of the Performance of HIPERLAN/2 and IEEE 802.11a Physical Layers', VTC Spring, May 2001.

[11] G. H. Golub and C. F. Van Loan, 'Matrix Computations', The John Hopkins University Press, 1996.

[12] M.K. Abdul Aziz, P.N. Fletcher and A.R. Nix, 'Performance analysis of IEEE 802.11n solutions combining MIMO architectures with iterative decoding and sub-optimal ML detection via MMSE and Zero forcing GIS solutions', WCNC, March 2004.